Solution structure and proposed binding mechanism of a novel potassium channel toxin κ-conotoxin PVIIA

Martin J Scanlon[1]*, David Naranjo[2], Linda Thomas[1], Paul F Alewood[1], Richard J Lewis[1] and David J Craik[1]

Background: κ-PVIIA is a 27-residue polypeptide isolated from the venom of *Conus purpurascens* and is the first member of a new class of conotoxins that block potassium channels. By comparison to other ion channels of eukaryotic cell membranes, voltage-sensitive potassium channels are relatively simple and methodology has been developed for mapping their interactions with small-peptide toxins. PVIIA, therefore, is a valuable new probe of potassium channel structure. This study of the solution structure and mode of channel binding of PVIIA forms the basis for mapping the interacting residues at the conotoxin–ion channel interface.

Results: The three-dimensional structure of PVIIA resembles the triple-stranded β sheet/cystine-knot motif formed by a number of toxic and inhibitory peptides. Subtle structural differences, predominantly in loops 2 and 4, are observed between PVIIA and other conotoxins with similar structural frameworks, however. Electrophysiological binding data suggest that PVIIA blocks channel currents by binding in a voltage-sensitive manner to the external vestibule and occluding the pore. Comparison of the electrostatic surface of PVIIA with that of the well-characterised potassium channel blocker charybdotoxin suggests a likely binding orientation for PVIIA.

Conclusions: Although the structure of PVIIA is considerably different to that of the αK scorpion toxins, it has a similar mechanism of channel blockade. On the basis of a comparison of the structures of PVIIA and charybdotoxin, we suggest that Lys19 of PVIIA is the residue which is responsible for physically occluding the pore of the potassium channel.

Addresses: [1]Centre for Drug Design and Development, University of Queensland, St. Lucia, 4072, Australia and [2]Department of Biophysics, Instituto de Fisiologia Celular, UNAM, AP 70-253, CP 04510, Mexico DF, Mexico.

*Corresponding author.
E-mail: m.scanlon@mailbox.uq.edu.au

Key words: charybdotoxin, electrophysiology, NMR spectroscopy, potassium-channel blockers

Received: **21 August 1997**
Revisions requested: **18 September 1997**
Revisions received: **13 October 1997**
Accepted: **15 October 1997**

Structure 15 December 1997, **5**:1585–1597
http://biomednet.com/elecref/0969212600501585

Introduction

Voltage-gated ion channels, which span eukaryotic plasma membranes, directly mediate the flow of monovalent and divalent ions (e.g. Na^+, K^+ and Ca^{2+}) that regulate the electrical and biochemical activity of cells. A mechanistic understanding of the factors which govern the conductance and selectivity of these channels, therefore, is of great importance. Like nearly all integral membrane proteins, however, the voltage-gated ion channels are poorly defined at the level of molecular structure. This is largely due to the fact that the nature of these membrane-bound proteins makes them difficult to study by crystallographic or NMR spectroscopic methods. One approach to this problem has been the use of small peptide toxins with well-defined structures as probes of the structure and function of ion channels [1–3].

The venoms from marine snails of the genus *Conus* are a rich source of such toxins [4]. Conotoxins are small (8–35 residues) conformationally constrained molecules which bind with high affinity and specificity to ion channels and receptors in the mammalian neuromuscular system [5]. Although conotoxins are remarkably diverse, both in terms of their sequence and pharmacological properties, many of these peptides fall into distinct structural and activity classes, namely the α, μ, δ and ω conotoxins, which specifically interact at acetylcholine, sodium (two sites) or calcium channels, respectively [6]. Conotoxins have also been classified on the basis of characteristic arrangements of cysteine residues which give rise to two-, three- and four-loop frameworks, the loops being defined by the backbone segments between cysteine residues. An individual structural class can contain multiple pharmacological families, such that the ω, μO and δ conotoxins, which target various subtypes of calcium channels or sodium channels, have four-loop frameworks with remarkably similar folds. Residue substitutions at critical positions in the sequence result in the formation of the required toxin surface for highly potent and selective interactions with their receptors.

The ability of conotoxins to distinguish between different receptor subtypes has made them indispensable tools to unravel many physiological processes. There has also been considerable interest in these toxins as structural probes,

because a knowledge of their three-dimensional structure may be used to map the functional surface of their respective receptors [1]. Several structures of conotoxins from different receptor-binding classes have now been reported [7–13]; however, their use as probes of receptor structure has been hampered by a lack of detailed experimental data on how they interact with their respective ion channels at the molecular level. For this reason, the recent identification of the toxin κ-conotoxin PVIIA in the venom of the piscivorous snail *Conus purpurascens* is an exciting development. PVIIA is a four-loop conotoxin that is active at vertebrate K^+ channels and has been shown to block K^+ conductance in oocytes expressing the cloned K^+ channel encoded by the *Shaker* locus in *Drosophila* [14]. By comparison to other ion channels of eukaryotic cell membranes, voltage-sensitive potassium channels (VSKCs) are relatively simple as they can be assembled from four identical subunits. Through the combined use of recombinant DNA manipulation of the channel sequences and high resolution electrophysiological analysis with peptide toxins, the gross architecture of the active site of K^+ channels is beginning to become apparent. It is known, for example, that VSKCs are tetramers organised in axial fourfold symmetry around the K^+-selective pore [15] and that the most crucial determinants of ion selectivity are found in a short stretch of sequence between the fifth and sixth transmembrane helical domains [16–18].

Studies with scorpion toxins have established methodology for defining the complementary interacting surfaces of the pore loops of VSKCs and peptide toxins of known structure [1–3]. Identification of new ion-channel probes with different binding surfaces and channel subtype specificity will aid in the improved characterisation of VSKCs. Recently, the structure [19] and binding surface [20] of a novel potassium channel toxin, ShK, from the sea anemone *Stichodactyla helianthus* have been reported. κ-Conotoxin PVIIA is significantly different, both in size and sequence, to either the αK scorpion toxins or sea anemone toxins and as such represents the first member of a new class of structural probes of VSKCs. The discovery of novel potassium channel ligands such as ShK and PVIIA will probably provide new insights into the structural factors that govern ion channel subtype specificity.

A knowledge of the structure of PVIIA is an essential prerequisite for binding studies aimed at gaining new topographical information about K^+ channels. Information obtained regarding its mode and orientation of binding to the potassium channel may facilitate the development of similar models of the voltage-sensitive sodium and calcium channels which are targeted by other conotoxins with similar structural frameworks.

In this study, we report the solution structure of PVIIA as well as preliminary electrophysiological data aimed at identifying its mechanism of action. These data suggest that PVIIA blocks the pore of the channel, but binding is mediated through a different set of complementary interactions than those observed with scorpion toxins. On the basis of a comparison of our structure of PVIIA with that of the αK scorpion toxin charybdotoxin (CTX), which binds to the outer vestibule of the Shaker K^+ channel and blocks ion currents by physically occluding the pore [21], we propose a mode of binding for PVIIA.

Results

Peptide synthesis

PVIIA was prepared by solid-phase peptide synthesis and the disulfide bonds formed by air oxidation in the presence of reduced and oxidised glutathione. The peptide was purified using analytical reverse-phase HPLC, and its purity and molecular weight were confirmed by electrospray ionisation mass spectrometry.

Resonance assignments

Resonances were assigned to specific protons using standard sequential assignment procedures [22]. Spectra recorded at different temperatures were used to confirm assignments in cases of peak overlap or coincidence with the water resonance. Figure 1 shows the fingerprint region of a DQF–COSY and a 250 ms mixing time NOESY spectrum recorded in 90% H_2O/10% ^2H_2O. A summary of the short and medium range NOE connectivities along with $^3J_{HNH\alpha}$ coupling constant and amide proton exchange data is presented in Figure 2.

Structure determination and analysis

Structures were generated using a restraint set consisting of 320 inter-proton distances inferred from NOE intensities, 21 backbone and 15 sidechain dihedral angles. Stereospecific assignments were made for ten β-methylene pairs along with all five pairs of sidechain amide protons of asparagine and glutamine residues. The inter-proton restraints, from which redundancies based on the covalent geometry had been eliminated, consisted of 64 intra-residue, 110 sequential, 58 medium-range and 88 long-range distances.

Initial structures were calculated in X-PLOR [23], using a dynamical simulated annealing protocol in a geometric force field. These were energy minimised using a modified CHARMm [24] force field. From the final round of calculations, a family of 20 structures (from a total of 50) with the lowest energies and least residual violations of the experimental restraints were chosen to represent the structure of PVIIA. A summary of the structural statistics for this family is given in Table 1. The structures have no violations of distance or dihedral angle restraints greater than 0.15 Å or 2°, respectively, they have good covalent geometry, as indicated by the small deviations from ideal bond lengths and bond angles, and they have favourable

Figure 1

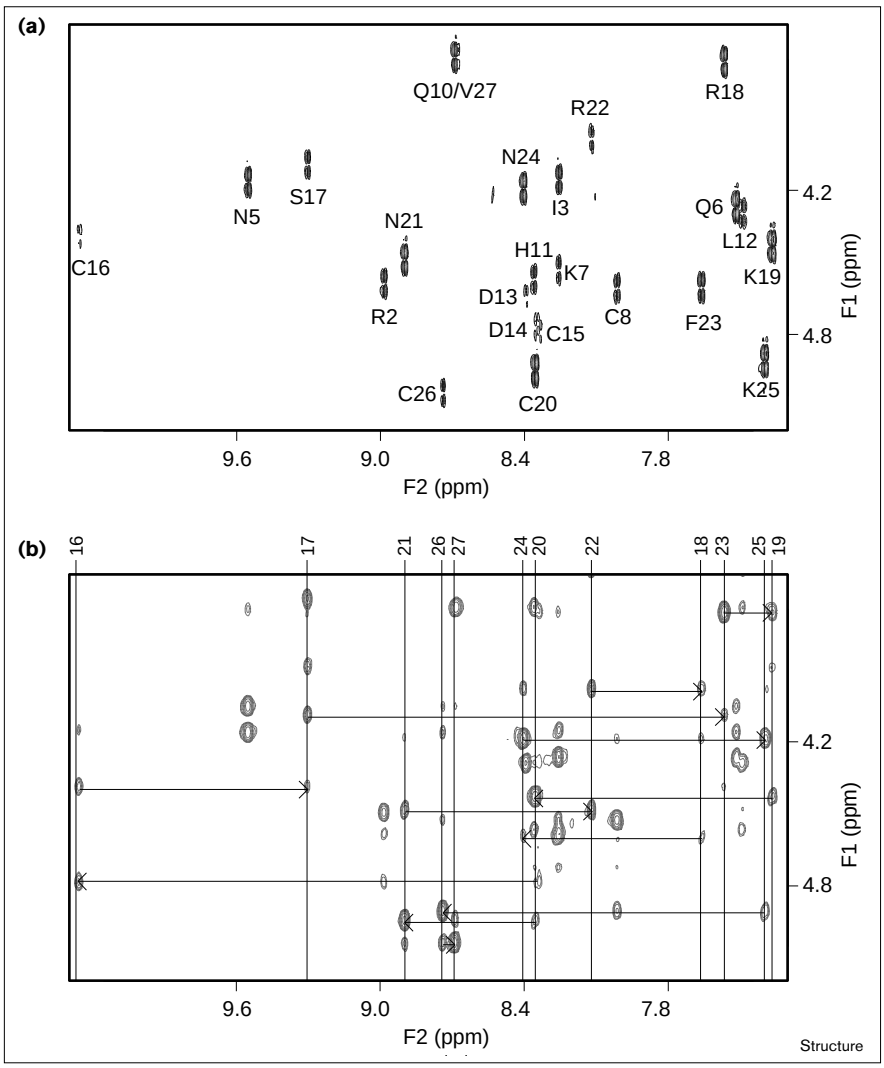

Fingerprint regions of NMR spectra of PVIIA. **(a)** DQF–COSY spectrum of PVIIA recorded in 90% H_2O/10% ^2H_2O at 750 MHz, 298K and pH 3.0. Cross peaks are labelled according to the one-letter amino acid code and numbers indicate the position in the sequence of PVIIA. **(b)** 250 ms mixing time NOESY spectrum recorded in 90% H_2O/10% ^2H_2O. Vertical lines indicate the amide proton resonance positions of residues 15–27 and sequential $H\alpha$–NH_{i+1} connectivities are shown by arrows for these residues.

non-bonded contacts, indicated by the low values of the mean Lennard–Jones potential.

The root mean square deviations (rmsds) for the coordinates of the backbone heavy atoms, when the final 20 structures are superimposed over the entire sequence, are shown as a function of residue number in Figure 3a. These data indicate that the structure is generally well defined, with the least ordered region being loop 2 (residues 9–14). Backbone angular order parameters (Figure 3b–c) are > 0.96 for the entire molecule and > 0.99 for all residues outside loop 2. Mean pairwise rmsds, over the whole molecule, for the backbone heavy atoms (N, Cα and C) and all heavy atoms are 0.38 (± 0.10) Å and 1.52 (± 0.19) Å, respectively. Corresponding values when loop 2 is excluded are 0.27 (± 0.08) Å and 1.40 (± 0.21) Å, respectively. The relative disorder in loop 2 is reflected in decreased sidechain order parameters (Figure 3d).

A stereoview of the final 20 structures superimposed over the backbone heavy atoms is shown in Figure 4. The positions of the three disulfide bonds, which make up the hydrophobic core of the molecule, are indicated. Analysis of the family of structures in PROCHECK [25] reveals that 73% of residues lie in the most favoured regions of the Ramachandran plot with the remaining 27% in the additionally allowed region.

Description of the structure

Elements of secondary structure were identified using the program PROMOTIF [26]. PVIIA contains three β strands, encompassing residues 6–8, 19–21 and 24–27. According to the criteria of Kabsch and Sander [27], these elements do not formally constitute a β sheet as there are only two hydrogen bonds present between each pair of strands as shown Figure 5. A similar structural element, however, has been identified in a number of other conotoxins and

Figure 2

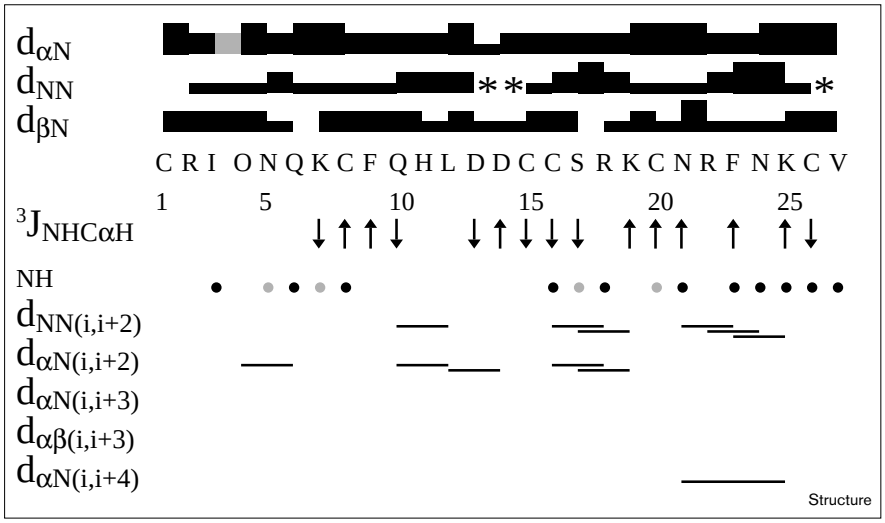

Summary of the NMR data used for sequence-specific assignments and identification of secondary structure in PVIIA. Shaded bars indicate sequential connectivities observed in a 250 ms mixing time NOESY spectrum at 298K and pH 3.0, with the height of the bars indicating their strength. Medium range connectivities are also shown. ↓ indicates values of $^3J_{HNH\alpha} \leq 5$ Hz; ↑ indicates values of $^3J_{HNH\alpha} \geq 8$ Hz. Grey circles indicate backbone NH protons that were still observed in TOCSY spectra of PVIIA 4 h after dissolution in ^2H_2O; black circles indicate backbone NH protons that were not fully exchanged after 24 h.

classified as an antiparallel triple stranded β sheet with +2x, –1 topology. An isolated β bridge involving Arg2 and Cys16 is also present, containing hydrogen bonds as shown in Figure 5.

Five β turns are present in the loops of PVIIA: residues Ile3–Gln6 form a type II β turn, residues Phe9–Leu12 and residues Gln10–Asp13 form overlapping type IV turns, and residues Cys15–Arg18 and Asn21–Asn24 form type I turns. A hydrogen bond was consistently found for the turns 3–6 and 21–24, in structures calculated in the absence of hydrogen-bonding restraints. In addition, an inverse γ-turn is present between residues Leu12–Asp14. In two of the final structures, the overlapping turns between Phe9–Asp14 are classified as a short stretch of 3_{10} helix.

Table 1

Statistics for the family of 20 PVIIA structures*.

Mean rmsd from experimental restraints	
NOE (Å)	0.0125 ± 0.00054
dihedrals (°)	0.43 ± 0.044
Mean rmsd from idealised covalent geometry†	
bonds (Å)	0.0075 ± 0.0003
angles (°)	2.20 ± 0.021
impropers (°)	0.152 ± 0.010
Restraint violations	
mean NOE violations per structure > 0.1 Å	1.3 ± 0.5
maximum NOE violation (Å)	0.13
mean dihedral angle violations per structure > 1°	2.5 ± 0.9
maximum angle violation (°)	1.84
Mean energies (kJ mol^{-1})	
E_{NOE}‡	2.05 ± 0.18
E_{cdih}‡	0.20 ± 0.04
E_{L-J}§	–154.27 ± 6.57
E_{bond}	3.70 ± 0.26
$E_{improper}$	0.49 ± 0.07
E_{angle}	56.6 ± 1.13
E_{total}	–84.7 ± 7.02

*The values in the table are given as means ± standard deviation. †Idealised geometry is defined by the CHARMm force field as implemented within X-PLOR. ‡Force constants for the calculation of square well potentials for the NOE and dihedral angle restraints were 50 kcal mol^{-1} Å^{-2} and 200 kcal mol^{-1} rad^{-2}, respectively. §The Lennard–Jones van der Waals energy was calculated with the CHARMm empirical energy function.

The elements of secondary structure identified in the calculated structures of PVIIA account reasonably well for the amide protons which were found to be in slow exchange with ^2H_2O. Only Ile3 and Arg18 lack clearly defined hydrogen-bonding partners, although in three of the final structures a hydrogen bond is present in the 15–18 β turn. A number of hydrogen bonds involving sidechain acceptors have also been identified and these include: Ser17 NH–Ser17 OG (19/20 structures), Lys19 NH–Ser17 OG (14/20 structures), Cys20 NH–Asp13 OD2 (8/20 structures), Phe23 NH–Asn20 OD1 (10/20 structures) and Lys25 NH–Asn20 OD1 (10/20 structures).

The Cys15–Cys26 disulfide bond forms a left-hand spiral (χSS = –88°, χ1/Cys15 = –43° and χ1/Cys26 = –75°), whereas the other two disulfide bonds have non-standard conformations (χSS = –77°, χ1/Cys1 = 100° and χ1/Cys16 = –149°; χSS = –127°, χ1/Cys8 = 59° and χ1/Cys20 = –70°). Like other four-loop conotoxins, the three disulfides in PVIIA form a cystine knot in which the Cys15–Cys26 bond passes through a ring formed by the other two disulfides and their connecting segments of the backbone.

Electrophysiology

Two-electrode voltage clamp (TEVC) recordings on whole oocytes were used to measure the effects of κ-conotoxin

Figure 3

Parameters for the family of 20 structures chosen to represent the solution conformation of PVIIA. **(a)** Rmsds from the average structure for the backbone heavy atoms (N, Cα and C). **(b–d)** Angular order parameters [8] for the backbone dihedral angles ϕ and ψ and the sidechain angle χ1.

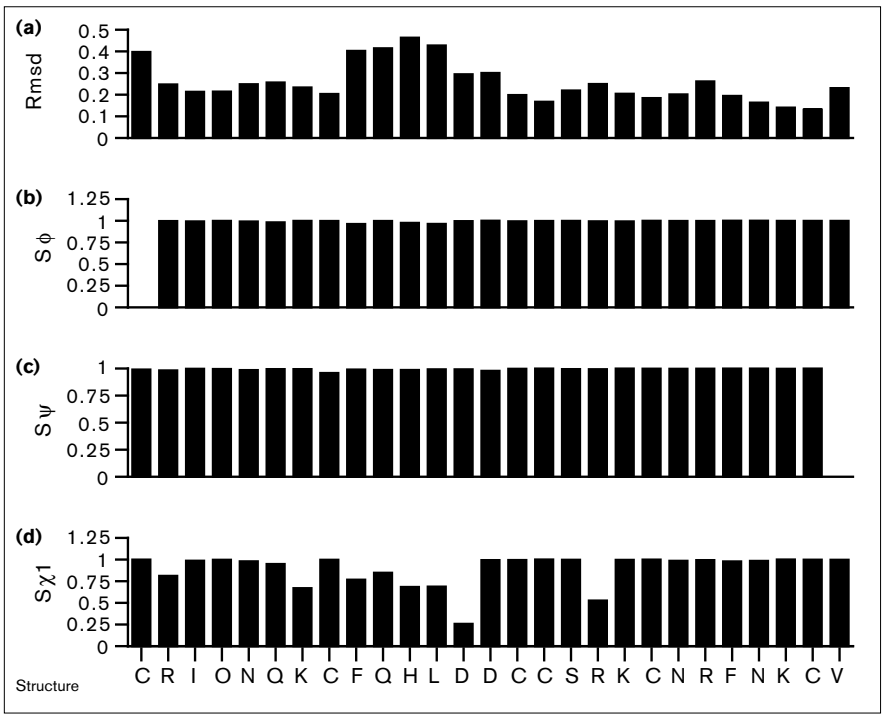

PVIIA on Shaker K^+ channel currents. To determine the effect of voltage on toxin blockade, currents were recorded as the oocytes were depolarised to increasingly positive voltages. Figure 6a shows the currents elicited in response to a series of depolarisations from a holding potential of –90 mV to –60 mV and in 10 mV steps to +50 mV in the absence of toxin. Figure 6b shows the same type of records when the experiments were recorded in the presence of 33 nM PVIIA. The apparent change in kinetics is due to relaxation of the voltage-dependent blockade as the command voltage is made more positive. The normalised inhibition time courses ($I_{PVIIA}/I_{control}$) were calculated from point-by-point division of the data in Figure 6b by the control family in Figure 6a and plotted (Figure 6c) to describe toxin inhibition. To avoid interference from activation kinetics, only those results obtained at voltages > 0 mV are shown. In order to undertake kinetic analysis of these data, it was necessary to modify the approach of Goldstein and Miller [21], to take account of the fast off-rate of PVIIA. The normalised data were fit to a single exponential function of the form:

$$f(t) = m–(m–n)*\exp(–t/\tau) \quad (1)$$

Equation 1 describes the relaxation of a first order (or pseudo-first order) equilibrium in response to a pulse-like perturbation: m is the asymptotic new equilibrium following the perturbation, n is the equilibrium state preceding the perturbation, t is the time after the perturbation and τ is the time constant of the current relaxation. Such an analysis is applicable to toxins with off-rates in the tens of millisecond timescale and allows resolution of kinetic processes that are faster than the solution exchange rate. The solid lines in Figure 6c correspond to a fit of the normalised inhibition time course to Equation 1. Note that the fitted lines converge at the beginning of the pulse, indicating the same level of prepulse inhibition. The time constants for current relaxation obtained from the solutions of this equation at different voltages were used to calculate the effective valence (zδ) of the voltage dependence according to Equation 2 ([21]; Figure 6d).

$$\tau = \tau(0)*\exp(z\delta FV/RT) \quad (2)$$

The values of zδ for PVIIA (0.48–0.55) are similar to the corresponding value for charybdotoxin (CTX; [21]) which indicates that blockade by PVIIA is similarly voltage sensitive. In CTX, the voltage sensitivity arises from the fact that the η-group of Lys27 interacts with potassium ions in the conduction pathway. Thus, a similar voltage dependency supports a similar mechanism of interaction for PVIIA.

If the mechanism of PVIIA blockade is indeed similar to that of the αK scorpion toxins, it would be expected that

Figure 4

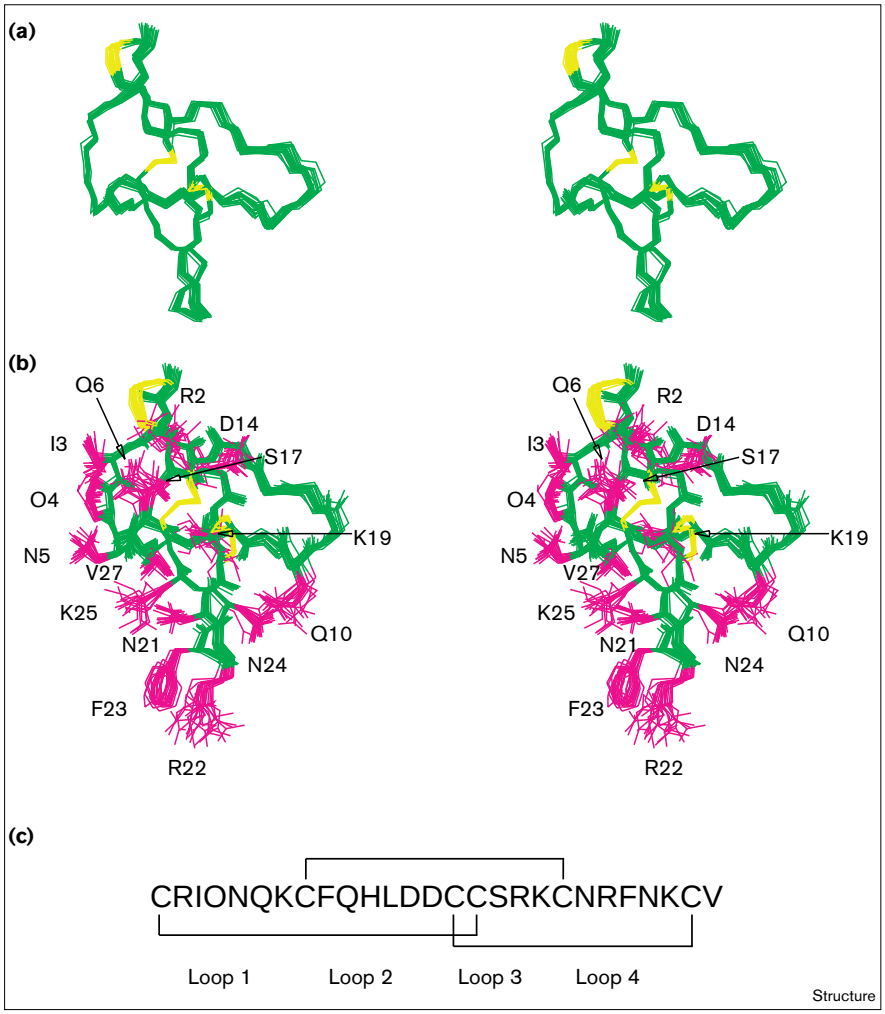

The solution structure of PVIIA. **(a)** Stereoview of the superimposed backbone heavy atoms (N, Cα and C) of the final 20 structures of PVIIA. The three disulfide bonds are shown in yellow. **(b)** Stereoview of the final structures in the same orientation. Backbone atoms (N, Cα and C) are shown in green, sidechain heavy atoms for the cysteine residues are shown in yellow and other well-defined sidechains ($S\chi1 > 0.8$) are shown in magenta. **(c)** The primary sequence and disulfide connectivity for PVIIA (O = γ-trans-L-hydroxyproline).

the tetraethylammonium ion (TEA), a specific K^+ channel pore blocker, would compete with PVIIA for binding, as is the case with CTX [28]. In order to test this hypothesis, toxin inhibition was studied by measuring whole cell currents in the presence and absence of external TEA. Figure 7a shows the currents elicited in response to a 100 ms depolarisation to 0 mV in the absence and presence of 100 nM PVIIA. Figure 7b shows the same type of records when the currents were recorded with 20 mM TEA in the external solution. In the absence of toxin, 20 mM TEA inhibited ~50% of the channel current at 0 mV, indicating that this concentration of TEA is close to its dissociation constant [28]. Normalised inhibition time courses are shown in Figure 7c. The continuous lines in Figure 7c are single exponential fits of the data to Equation 1, in which the time constants are 40 ms and 32 ms for 0 and 20 mM TEA, respectively. Addition of 20 mM TEA to the extracellular solution resulted in a ~50% weaker inhibition produced by 100 nM PVIIA. For the data shown in Figure 7c, apparent dissociation constants for PVIIA were calculated by measuring ($I_{PVIIA}/I_{control}$) values at the end of the 100 ms depolarisation pulse (using Equation 3), and they were found to be 360 and 700 nM in the absence and presence of TEA (20 mM), respectively.

$$I_{PVIIA}/I_{control} = \{1+[PVIIA]/K_d\}^{-1} \quad (3)$$

On average, with depolarisations to 0 mV, 20 mM TEA increased the apparent K_d of PVIIA by 2.3 ± 0.23 (mean ± sd; n = 3 separate experiments). These values are consistent with a competitive scheme in which the apparent K_d for the toxin is expected to be doubled when the concentration of its competitor is near its own K_d.

Discussion

The ability of conotoxins to distinguish between different receptor subtypes has resulted in their widespread

Figure 5

Schematic diagram of the secondary structural elements in PVIIA showing NOEs between β strands (double headed arrows) and the position of proposed hydrogen bonds (broken lines).

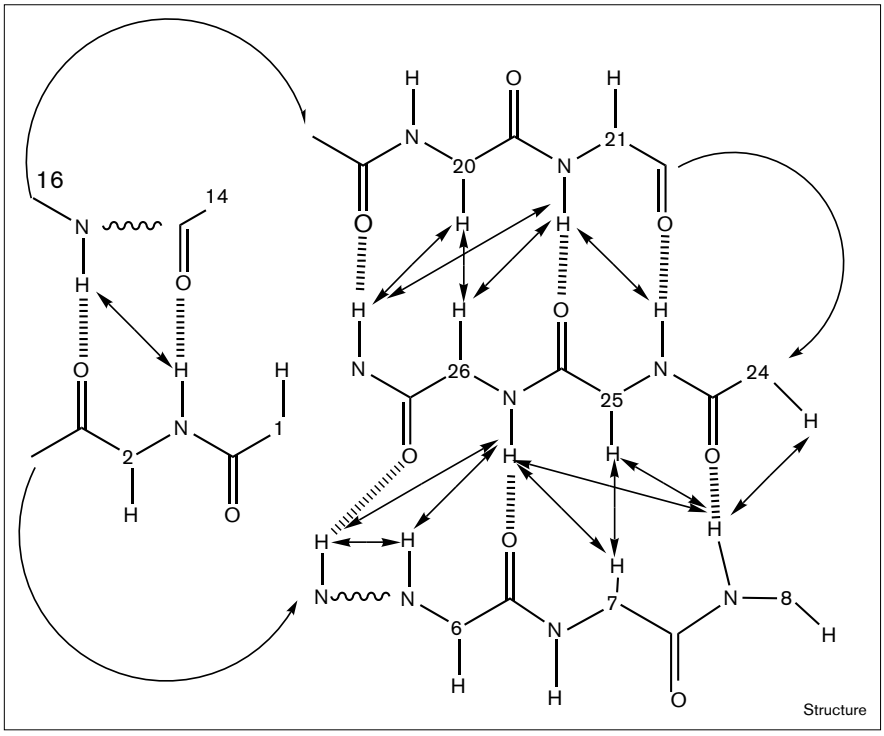

use as pharmacological probes of ion channels. For the same reasons, conotoxins have the potential to be used as templates for the development of ion channel therapeutics which combine high affinity with low toxicity. Detailed

Figure 6

Two-electrode voltage clamp (TEVC) records of currents elicited in response to a series of depolarisations from a holding potential of −90 mV to −60 mV and in 10 mV steps to +50 mV in the absence **(a)** and presence **(b)** of 33 nM PVIIA. **(c)** Point by point division of the data recorded in the presence of toxin (b) by the control family (a). The panel only shows those results obtained at voltages > 0 mV to avoid interference from activation kinetics. **(d)** Voltage dependency of the relaxation time constant obtained from the traces in (c).

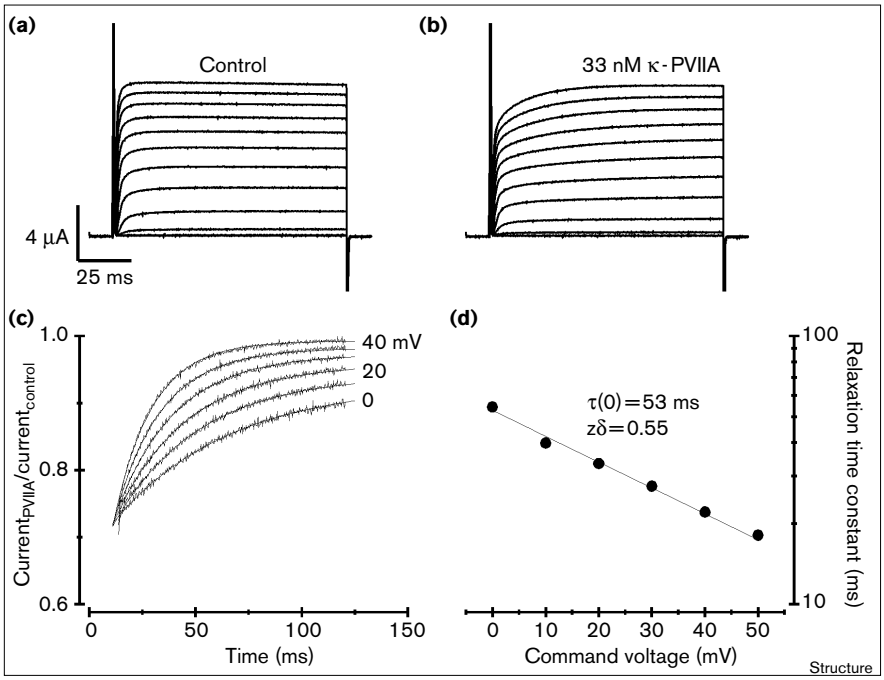

Figure 7

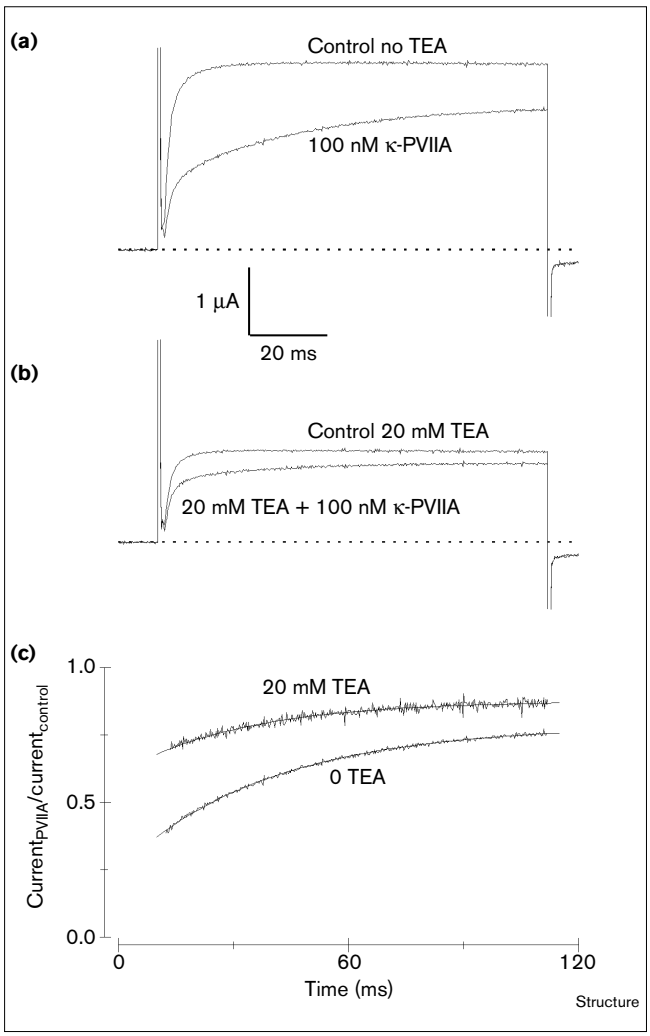

Toxin inhibition in the presence of TEA. **(a)** TEVC records of currents elicited in response to a 100 ms depolarisation to 0 mV under control conditions and in the presence of 100 nM PVIIA. **(b)** The same records measured after addition of TEA (20 mM) to the extracellular solution. **(c)** Normalised inhibition time course in the presence and absence of 20 mM TEA.

experimental data on how individual conotoxins interact with ion channels is currently lacking, however.

PVIIA is a recently identified conotoxin, found in the venom of the piscivorous snail *C. purpurascens*, which binds at nM concentrations to the Shaker K^+ channel [14]. This is the first conotoxin that has been identified with K^+ channel activity and as such represents the first member of the κ-class of conotoxins.

We have determined the structure of PVIIA at high resolution as a starting point from which to identify the residues necessary for high affinity interaction with the Shaker channel. PVIIA belongs to the four-loop class of conotoxins, containing six cysteine residues which form three disulfide bonds. This structural class displays diverse pharmacological activities and includes PVIIA, ω-conotoxins that block calcium channels, δ-conotoxins that delay the inactivation of sodium channels and conotoxin GS that blocks sodium channels. Solution structures have been previously reported for several ω-conotoxins [8,9,13] and conotoxin GS [12], which all share the same topology, comprising a triple stranded antiparallel β sheet with +2x, –1 topology linked by a cystine knot. This structural motif has now been reported for a number of toxic and inhibitory peptides [12,13,29–31].

Comparison of the structures of κ-PVIIA with ω-GVIA and conotoxin GS reveals that despite differences in the three sequences, the overall fold is remarkably similar (Figure 8). Indeed, the six Cα atoms of the conserved cysteine residues superimpose with an rmsd of 0.97 Å between ω-GVIA and κ-PVIIA and 1.27 Å between conotoxin GS and κ-PVIIA. The most notable differences between the three structures are in the size and relative orientation of loops 2 and 4. These structural differences are of particular interest because loop 2 of the ω-conotoxins is thought to be involved in calcium-channel binding and subtype discrimination [13]. Although the electrostatic profiles presented by the binding surfaces of the different conotoxins is likely to be the principal determinant of their specificity, the importance of the conformational differences observed among different classes of conotoxins is currently unclear. Without a knowledge of the binding orientation of the toxins on their respective channels and the mechanism of channel blockade, however, it is difficult to speculate on the importance of the observed structural differences.

We have investigated the binding of PVIIA to Shaker K^+ channels using electrophysiology and find that TEA ions compete with PVIIA and blockade by PVIIA is voltage sensitive. Although this result is apparently in conflict with those of Terlau *et al.* [14], we believe that this is due to their use of a channel with an attached inactivation domain. Inactivation kinetics mask the change in the toxin's binding affinity, which occurs as the membrane is stepped to depolarising potentials to open the channels. Furthermore, mutations in the K^+ channel vestibule were found to affect the binding affinity of PVIIA. For example, the channel mutation Lys427Glu increased toxin affinity by ~fivefold (data not shown). These results also indicate that the binding specificity of PVIIA is different to that of CTX. The affinity of CTX for the Shaker channel is increased > 2000-fold by the channel mutation Phe425Gly [32]; however, the same channel mutation makes PVIIA binding undetectable up to 5 μM. Taken together, these data strongly suggest that, like a number of αK scorpion toxins, PVIIA binds to

Figure 8

Comparison of the solution structures of **(a)** ω-conotoxin-GVIA **(b)** κ-conotoxin-PVIIA and **(c)** conotoxin-GS. The structures were aligned by superimposition over the Cα atoms of the six conserved half cysteines. Backbone heavy atoms (N, Cα and C) as well as the sidechain heavy atoms of the cysteine residues (yellow) are shown. Coordinates for GVIA (PDB accession code 1OMC; [9]) were obtained from the PDB. Coordinates for GS (PDB accession code 1AG7) were kindly provided by Justine Hill.

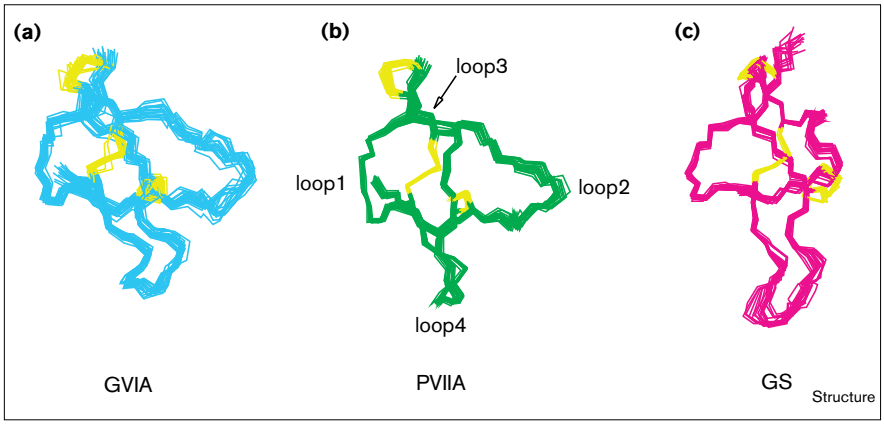

the external vestibule of the Shaker channel and blocks currents by physically occluding the pore.

Several studies have been reported that reveal details of interactions between CTX and the Shaker channel; therefore, a comparison of the structures of CTX and PVIIA represents a logical starting point from which to identify the possible orientation for PVIIA binding. Scanning mutagenesis experiments with CTX have revealed that binding is mediated by electrostatic interactions between the toxin and the channel [33]. CTX mutants in which each of the nine charge bearing residues were individually neutralised have revealed that only three charged residues, Arg25, Lys27 and Arg34, are crucial for toxin binding and blockade [34]. In addition, residues Lys11 and Lys31 in CTX have been shown to have unfavourable electrostatic interactions with the positively charged channel residue Lys427. The mutation Lys427Glu increases the affinity of CTX for the Shaker channel by ~50-fold [35]. Furthermore, Lys27 directly interacts with K^+ ions in the pore of the Shaker channel, conferring high affinity binding and voltage dependency to the dissociation rate [21]. Substitution of this residue for an arginine results in a marked reduction in affinity, while neutralisation of Lys27 to asparagine or glutamine drastically reduces the voltage sensitivity [21]. As PVIIA displays a similar voltage dependency of blockade to that of CTX, it would be expected that one of the three lysine residues in PVIIA binds within the pore of the channel and contributes significantly to the affinity of the interaction.

Comparison of the structure of PVIIA with that of CTX reveals a remarkable similarity in their folds (Figure 9a). CTX has a βαβ structure consisting of a triple-stranded antiparallel β sheet in which the first and second strands are linked by a loop containing an α helix. The residues that interact with the pore region of the K^+ channel are located on the second and third β strands and at the end of the α helix, which together form a relatively flat surface on one side of the molecule. Lys27, the residue which occludes the pore of the channel, is located on the second β strand. PVIIA, which also contains a triple-stranded antiparallel β sheet, has a considerably shorter sequence than CTX and lacks the α helix between the first and second β strands. As shown in Figure 9a, there is a striking similarity between CTX and PVIIA in the backbone fold of the remainder of the molecule, however. Furthermore, as shown in Figure 9b, when the backbone of Lys19 in PVIIA is superimposed over Lys27 in CTX, a number of positively charged residues in PVIIA align with positive charges in CTX that mediate binding to the Shaker channel. In this orientation, like CTX, PVIIA presents a flat surface which appears to be a prerequisite for toxins, interacting within the flat floor of the vestibule of the K^+ channel, to block ion flow. The majority of residues which contribute to this surface are contained in loop 4 of PVIIA, suggesting that the observed structural differences between conotoxins from different pharmacological classes may have functional significance. In this orientation, the sidechain of Lys19 in PVIIA overlaps that of Lys27 in CTX. Lys19 is therefore the residue which we suggest binds in the pore and confers voltage dependency to blockade of channel currents by PVIIA.

This model for PVIIA binding to the Shaker K^+ channel can now be used to direct a rational approach to mutational analysis aimed at identifying interacting pairs of residues on PVIIA and the Shaker channel. As we have demonstrated, the specificity of PVIIA is clearly different to that of any of the previously identified scorpion toxins. It is expected, therefore, that the data obtained from such mutational studies will enhance the currently available models of the selectivity-determining pore of the K^+ channel vestibule.

Figure 9

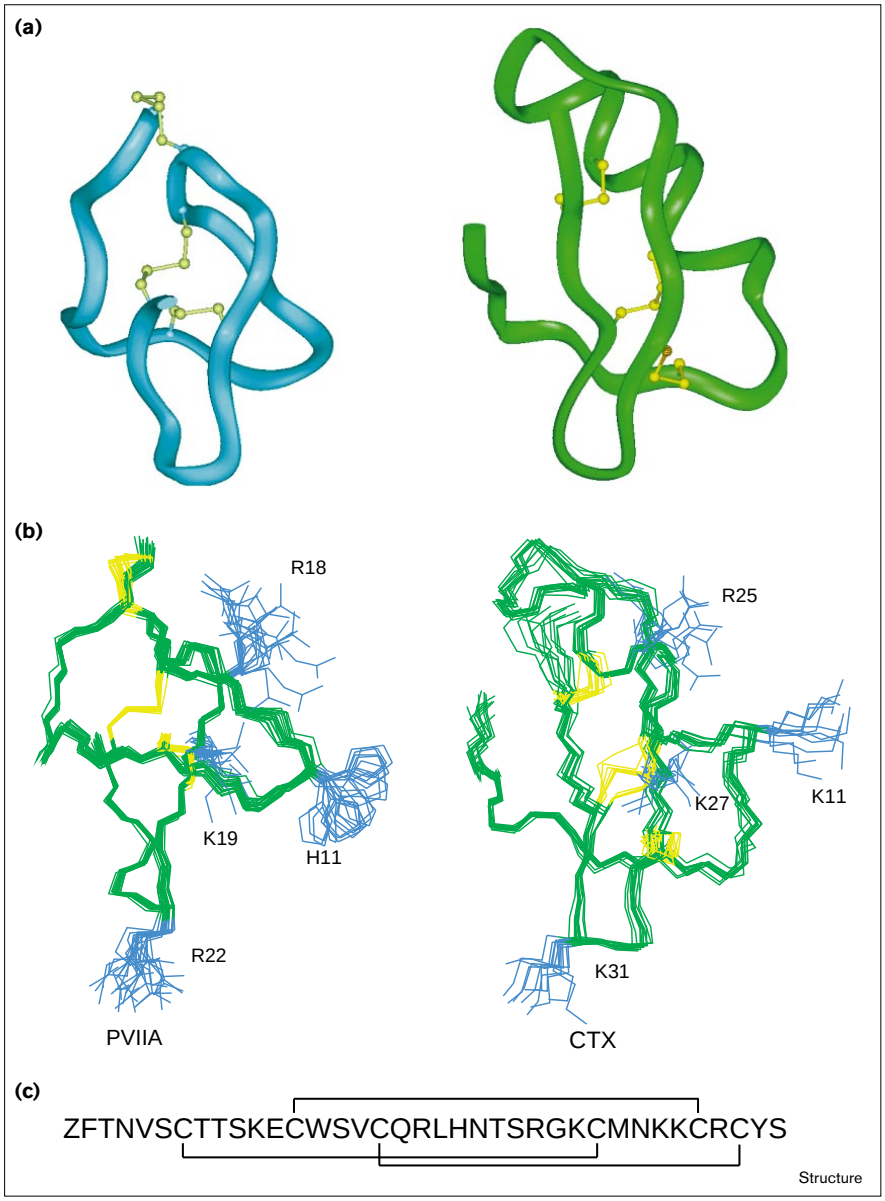

A comparison of the structures of PVIIA and CTX. **(a)** Comparison of Cα ribbon representations of the structures of PVIIA (blue) and CTX (green). Sidechain heavy atoms of the cysteine residues are shown in yellow. **(b)** Comparison of the structures of PVIIA and CTX. The alignment is based on superposition of the backbone heavy atoms (N, Cα and C) of Lys19 of PVIIA and Lys27 of CTX. Positively charged sidechains of CTX which have been found to mediate binding to the Shaker channel are shown in blue, as are selected positively charged sidechains of PVIIA. **(c)** The primary sequences and disulfide connectivity of charybdotoxin (Z = pyroglutamate).

Biological implications

Venomous marine snails of the genus *Conus* produce many small, disulfide-rich, peptide toxins with potent biological activities. Several of these conotoxins have been found to be highly selective blockers of mammalian ion channels. Such channels control a variety of biological processes and represent important therapeutic targets. Like other membrane proteins, however, ion channels are beyond the scope of direct structure determination by currently available methods. One solution to this problem has been the use of small molecules with well-defined structures to probe the complementary structure of their receptors. Although conotoxins would seem to be ideal for this purpose, their use as structural probes has been hampered by a lack of detailed experimental data on how they interact with their respective ion channels at the molecular level.

In this study, we have determined the structure of κ-conotoxin PVIIA. PVIIA is the first member in a new class of conotoxins that block voltage-sensitive potassium channels (VSKCs). By comparison to other ion channels of eukaryotic cell membranes, VSKCs have relatively simple architecture and a methodology has been devised for mapping their interactions with small peptide toxins. Our electrophysiological data for PVIIA

suggest that it binds to the external vestibule of the Shaker K+ channel and blocks currents by physically occluding the pore. Furthermore, blockade by PVIIA has similar voltage dependency to blockage by charybdotoxin (CTX). Comparison of the structures of PVIIA and CTX suggest a likely binding orientation in which Lys19 of PVIIA is the residue which confers voltage dependency to the channel blockage. In this orientation, PVIIA binding to the outer vestibule of the Shaker K+ channel is mediated through a different set of interactions to those of previously characterised toxins. Identification of those residues on the surface of PVIIA that interact with the VSKC, therefore, will enhance current models of the channel pore.

Knowledge of the structural basis for channel blockade by PVIIA may assist in the development of similar models describing blockade of voltage-sensitive sodium and calcium channels that are targeted by other conotoxins with the same structural framework. Such models should prove useful as guides to the development of novel selective and therapeutically useful ion channel modulating agents.

Materials and methods

Peptide synthesis

Boc-L-amino acids were obtained from Novabiochem (Läufelfingen, Switzerland) or the Peptide Institute (Osaka, Japan); t-Boc-Val-OCH_2-PAM-resin (substitution value 0.77 mmol g^{-1}) was obtained from Perkin Elmer (Brisbane, Australia). 2-(1H-benzotriazol-1-yl)-1,1,3,3,-tetramethyluronium hexafluorophosphate (HBTU) was obtained from Richelieu Biotechnologies (Quebec, Canada). Other reagents were of peptide synthesis grade from Auspep (Melbourne, Australia).

Stepwise synthesis (0.5 mmol scale, 0.649 g resin) was conducted manually using *in situ* BOC SPPS [36], starting from Boc-PAM-Val resin. The average coupling was 99.80 as determined by ninhydrin assay [37]. The peptide was cleaved from the resin using HF:*p*-cresol:*p*-thiocresol (18:1:1) at −10–0°C for 1 h. Peptide was precipitated with cold ether, collected by filtration on a sinter funnel, washed with cold ether and dissolved in 50% AcOH, diluted with water and lyophilised. The crude peptide was purified by preparative chromatography (Vydac C18 column, 2.2 × 25 cm), using a 1% gradient (100% A to 80% B, 80 min; A = 0.1% TFA in H_2O, B = 0.09% TFA, 10% H_2O, 90% CH_3CN) to give reduced peptide in 34% yield.

The folded product was obtained by dissolving reduced peptide (10 mg) in aqueous 0.33 M NH_4OAc/0.5 M GnHCl (154 ml), with pH adjusted to 7.8 using 0.01 M NH_4OH. The solution was stirred at 4°C for 5 days, in the presence of reduced and oxidised glutathione (molar ratio of peptide:GSH:GSSG was 1:100:10). The oxidation was terminated by lowering the pH to 2–3 with TFA (5 ml). The reaction mixture was loaded onto a preparative HPLC column (Vydac C18 column, 2.2 × 25cm) (8 ml min^{-1}) and washed with 0.1% TFA until all oxidation buffer had eluted. A 1% gradient (100% A to 80% B, 80 min) was applied and pure oxidised κ-PVIIA was isolated in 95% yield. Electrospray ionisation mass spectra recorded on a PE Sciex API III triple quadrupole mass spectrometer were used to confirm the purity and molecular weights of the synthetic peptides.

NMR Spectroscopy. NMR samples contained ~1.5 mM peptide in either 90% H_2O/10% ^2H_2O or ^2H_2O at pH 3.0. pH values are meter readings at 295K, uncorrected for deuterium isotope effects. Spectra were recorded on a Bruker DRX 750 spectrometer with sample temperatures of 280K, 298K or 313K. In all experiments, the carrier was set at the centre of the spectrum on the water resonance frequency and quadrature detection was used in both dimensions. Spectra were recorded in phase sensitive mode using TPPI [38]. The following homonuclear 2D NMR spectra were recorded: double quantum filtered (DQF) COSY [39], TOCSY [40] with MLEV17 [41] isotropic mixing periods of 50 and 80 ms, ECOSY [42] and NOESY [43] with mixing times of 80 ms, 150 ms and 250 ms. Water suppression was achieved using selective low power irradiation of the water resonance during the relaxation delay of 1.8 s and during the mixing period in NOESY experiments. Slowly exchanging amide protons were identified by recording a series of 1D and TOCSY spectra on a fully protonated sample of PVIIA immediately following dissolution in ^2H_2O.

Spectra were processed on a Silicon Graphics Indigo 2 R8000 using UXNMR (Bruker). Data were processed as described previously [13]. Processed data were analysed using AURELIA (Bruker) and plots for the figures were generated using Felix 2.3 (Biosym).

Structure calculations

Distance constraints were derived from the intensity of cross peaks in NOESY spectra recorded in 90% H_2O/10% ^2H_2O and ^2H_2O with a mixing time of 250 ms. Cross peaks were classified as strong, medium, weak or very weak and assigned corresponding upper bounds of 2.7 Å, 3.5 Å, 5.0 Å or 6.0 Å, respectively. Pseudoatom corrections were added to distance constraints where necessary and a further 0.5 Å was added to the upper bound of restraints involving methyl protons.

Backbone dihedral φ angles were derived from $^3J_{HNH\alpha}$ coupling constants measured from either 1D NMR spectra or from lineshape analysis of the antiphase crosspeak splitting in a high digital resolution 2D DQF–COSY spectrum. Dihedral angle constraints were applied as follows: −120° ± 30° for $^3J_{HNH\alpha} > 8$ Hz; −60° ± 30° for $^3J_{HNH\alpha} < 5$ Hz. Additional f angle restraints of −100° ± 80° were applied in cases where the intra residue dαN(i,i) NOE was clearly weaker than the sequential dαN(i,i+1) NOE.

Positive φ angle restraints of +60° ± 30° were used for residues where 6 Hz $< {}^3J_{HNH\alpha} <$ 8 Hz and the intra residue dαN(i,i) NOE was strong. In preliminary structure calculations, in which no positive φ angle restraints were included, these residues angles converged to a positive value in the majority of cases.

Stereospecific assignment of the β-methylene protons and χ1 dihedral angle restraints were derived using $^3J_{\alpha\beta}$ coupling constants measured form ECOSY spectra, together with dαβ(i,i) and dNβ(i,i) NOE intensities [44]. χ1 angles were restrained to values of 60°, 180° or −60°, as appropriate, with a range of ± 30°. Additional χ1 restraints were obtained for Ile3 and Val27 from measurement of $^3J_{\alpha\beta}$ in the ECOSY spectrum.

Structures were calculated using a dynamic simulated annealing protocol in X-PLOR 3.1 [23] using a geometric force field. Starting structures were generated using random (φ,ψ) dihedral angles and energy minimised (500 steps) to produce structures with the correct local geometry. A soft square well potential [45] was used for NOE and dihedral constraints and bond lengths were fixed during the high temperature and cooling stages. The structures were subjected to 30 ps of high temperature molecular dynamics at 1000 K before cooling to 0 K and final energy minimisation over 15 ps. Structure refinements were performed using energy minimisation under the influence of the CHARMm forcefield [24].

The final 20 structures with the lowest overall energies which had no violations of NOE restraints > 0.15 Å or dihedral angle restraints > 2.0° were retained for analysis. Structures were visualised using InsightII (Biosym) and analysed using the program PROMOTIF [26].

Molecular biology

In vitro cRNA synthesis and expression of Shaker channel mutants Phe425Gly and Lys427Glu were undertaken as described by Goldstein *et al.* [34].

Electrophysiology

Oocytes from *Xenopus laevis* were injected with 0.05–0.5 ng of total RNA [32], coding for the inactivation removed Shaker K^+ channel (Δ6–46) [46]. Currents were recorded using two electrode voltage clamp (TEVC) recordings on whole oocytes at room temperature [47]. Extracellular solution consisted of 96 mM NaCl, 2 mM KCl, 0.3 mM $CaCl_2$, 10 mM HEPES (pH 7.6) and bovine serum albumin (25 mg ml^{-1}). Current and voltage electrode pipettes (0.2–0.5 MΩ) were filled with a solution of 3 mM KCl, 5 mM EGTA and 10 mM HEPES (pH 7.0). During the experiments the oocytes were maintained at a holding potential of −90 mV. TEVC records were obtained of currents elicited in response to 100 or 110 ms depolarisations to −60 mV to +50 mV in 10 mV steps. The time course of toxin inhibition was obtained from point-by-point division of records obtained in the presence of PVIIA (33–100 nM) from control records obtained in its absence. Kinetic analysis of these time courses was undertaken by fitting the data to a single exponential function (equation 1) as described in the text.

To determine the effect of external TEA ions on channel blockade, experiments were undertaken, essentially as described above, in the absence and presence of PVIIA and repeated after the addition of TEA (20 mM) to the extracellular solution. Apparent dissociation constants (K_d) for PVIIA were estimated from the standard one-site inhibition equation, given by Equation 3.

In the presence of TEA, the toxins apparent K_d is given by:

$$K_d = K_{d(0)} * \{1 + [TEA]/K_{d(TEA)}\} \quad (4)$$

in which $K_{d(0)}$ is the dissociation constant in the absence of TEA.

Accession numbers

Coordinates for PVIIA have been submitted to the Protein Data Bank with the accession code 1AV3.

Supplementary material

The supplementary material available with the Internet version of this paper contains a table of Chemical shift assignments (ppm) for PVIIA in 90% H_2O/10% ^2H_2O at 298K and pH 3.0.

Acknowledgements

This work was supported in part by a grant from the Australian Research Council to DJC. DN was partially supported by grant DGAPA–UNAM IN200397. We thank Chris Miller for helpful discussions and allowing parts of this work to be undertaken in his laboratory.

References

1. Miller, C. (1995). The charybdotoxin family of K^+ channel blocking peptides. *Neuron* **15**, 5–10.
2. Aiyar, J., *et al.*, & Chandy, K.G. (1995). Topology of the pore region of a K^+ channel revealed by the NMR-derived structures of scorpion toxins. *Neuron* **15**, 1169–1181.
3. Ranganathan, R., Lewis, J.H. & Mackinnon, R. (1996). Spatial localisation of the K^+ channel selectivity filter by mutant cycle-based structure analysis. *Neuron* **16**, 131–139.
4. Bingham, J.P., Jones, A., Lewis, R.J., Andrews, P.R. & Alewood, P.F. (1996). *Conus* venom peptides (conopeptides): inter-species, intra-species and within individual variation revealed by ionspray mass spectrometry. In *Biochemical Aspects of Marine Pharmacology*, (Lazarovici, P., ed.), pp 13–27, Alaken, Colorado.
5. Myers, R.A., Cruz, L.J., Rivier, J.E. & Olivera, B.M. (1993). *Conus* peptides as chemical probes for receptors and ion channels. *Chem. Rev.* **93**, 1923–1936.
6. Lewis, R.J., *et al.*, & Andrews, P. (1996). Secrets of the cone shell. *Life Sci.* **8**, 16–24.
7. Ott, K.H., Becker, S., Gordon, R.D. & Rüterjans, H. (1991). Solution structure of μ-conotoxin GIIIA analysed by 2D-NMR and distance geometry calculations. *FEBS Letters* **278**, 160–166.
8. Pallaghy, P.K., Duggan, B.M., Pennington, M.W. & Norton, R.S. (1993). Three-dimensional structure in solution of the calcium channel blocker ω-conotoxin. *J. Mol. Biol.* **234**, 405–420.
9. Davis, J.H., Bradley, E.K., Miljanich, G.P., Nadasdi, L., Ramachandran, J. & Basus, V.J. (1993). Solution structure of ω-conotoxin GVIA using 2-D NMR spectroscopy and relaxation matrix analysis. *Biochemistry* **32**, 7396–7405.
10. Farr-Jones, S., Miljanich, G.P., Madasdi, L., Ramachandran, J. & Basus, V.J. (1995). Solution structure of ω-conotoxin MVIIC, a high affinity ligand of P-type calcium channels using ^1H NMR spectroscopy and complete relaxation matrix analysis. *J. Mol. Biol.* **248**, 106–124.
11. Hill, J.M., Alewood, P.F. & Craik, D.J. (1996). Three-dimensional solution structure of μ-conotoxin GIIIB, a specific blocker of skeletal muscle sodium channels. *Biochemistry* **35**, 8824–8835.
12. Hill, J.M., Alewood, P.F. & Craik, D.J. (1997). Solution structure of the sodium channel antagonist conotoxin GS: a new molecular calliper for probing sodium channel geometry. *Structure* **5**, 571–583.
13. Nielsen, K.J., Thomas, L., Lewis, R.J., Alewood, P.F. & Craik, D.J. (1996). A consensus structure for ω-conotoxins with different selectivities for voltage sensitive calcium channel subtypes: comparison of MVIIA, SVIB and SNX-202. *J. Mol. Biol.* **263**, 297–310.
14. Terlau, H., Shon, K.-J., Grilley, M., Stocker, M., Stühmer, W. & Olivera, B.M. (1996). Strategy for rapid immobilisation of prey by a fish-hunting marine snail. *Nature* **381**, 148–151.
15. Mackinnon, R. (1991). Determination of the subunit stoichiometry of a voltage-activated potassium channel. *Nature* **350**, 232–235.
16. Miller, C. (1991). 1990: *Annus mirabilis* of potassium channels. *Science* **252**, 1092–1096.
17. Sigworth, F.J. (1994). Voltage gating of ion channels. *Quart. Rev. Biophys.* **27**, 1–40.
18. Mackinnon, R. (1995). Pore loops: an emerging theme in ion channel structure. *Neuron* **14**, 889–892.
19. Tudor, J.E., Pallaghy, P.K., Pennington, M.W. & Norton, R.S. (1996). Solution structure of ShK toxin, a novel potassium channel inhibitor from a sea anemone. *Nature Struct. Biol.* **3**, 317–320.
20. Pennington, M.W., Mahnir, V.M., Khaytin, I., Zaydenburg, I., Byrnes, M.E. & Kem, W.R. (1996). An essential binding surface for ShK toxin interaction with rat brain potassium channels. *Biochemistry* **35**, 16407–16411.
21. Goldstein, S.A.N. & Miller, C. (1993). Mechanism of charybdotoxin block of a voltage-gated K^+ channel. *Biophys. J.* **65**, 1613–1619.
22. Wüthrich, K. (1986). *NMR of proteins and nucleic acids*. John Wiley & Sons Inc., New York.
23. Brünger, A.T. (1992). *X-PLOR Version 3.1. A system for X-ray crystallography and NMR*. Yale University Press, New Haven, CT.
24. Brooks, B.R., Bruccoleri, R.E., Olafson, B.D., States, D.J., Swaminathan, S. & Karplus, M. (1983). CHARMm: A program for macromolecular energy minimisation and dynamics calculations. *J. Comp. Chem.* **4**, 187–217.
25. Laskowsi, R.A., MacArthur, M.W., Moss, D.S. & Thornton, J.M. (1993). PROCHECK: a program to check the stereochemical quality of protein structure coordinates. *J. Appl. Cryst.* **26**, 283–291.
26. Hutchinson, E.G. & Thornton, J.M. (1996). PROMOTIF: a program to identify and analyse structural motifs in proteins. *Protein Sci.* **5**, 212–220.
27. Kabsch, W. & Sander, C. (1983). Dictionary of protein secondary structure: pattern recognition of hydrogen-bonded and geometrical features. *Biopolymers* **22**, 2577–2637.
28. Miller, C. (1988). Competition for block of a Ca^{2+} activated K^+ channel by charybdotoxin and tetraethylammonium. *Neuron* **1**, 1003–1006.
29. Pallaghy, P.K., Nielsen, K.J., Craik, D.J. & Norton, R.S. (1994). A common structural motif incorporating a cystine knot and a triple-stranded β-sheet in toxic and inhibitory peptides. *Protein Sci.* **3**, 1833–1839.
30. Narasimhan, L., Singh, J., Humblet, C., Guruprasad, K. & Blundell, T. (1994). Snail and spider toxins share a similar tertiary structure and 'cystine motif'. *Nat. Struct. Biol.* **1**, 850–852.
31. Fletcher, J.L., *et al.*, & King G.F. (1997). The structure of a novel insecticidal neurotoxin, atracotoxin-HVI, from the venom of an Australian funnel web spider. *Nat. Struct. Biol.* **4**, 559–566.
32. Goldstein, S.A.N. & Miller, C. (1992). A point mutation in a *Shaker* K^+ channel changes its charybdotoxin binding site from low to high affinity. *Biophys. J.* **62**, 5–7.

33. Park, C.S. & Miller, C. (1992). Mapping function to structure in a channel-blocking peptide: electrostatic mutants of charybdotoxin. *Biochemistry* **31**, 7749–7755.
34. Goldstein, S.A.N., Pheasant, D.J. & Miller, C. (1994). The charybdotoxin receptor of a *Shaker* K^+ channel: peptide and channel residues mediating molecular recognition. *Neuron* **12**, 1377–1388.
35. Stocker, M. & Miller, C. (1994). Electrostatic distance geometry in a K^+ channel vestibule. *Proc. Natl. Acad. Sci. USA* **91**, 9509–9513.
36. Schnolzer, M., Alewood, P.F., Jones, A., Alewood, D. & Kent, S.B.H. (1992). *In situ* neutralisation in Boc-chemistry solid phase peptide synthesis. *Int. J. Pept. Protein Res.* **40**, 180–193.
37. Sarin, V., Kent, S.B.H., Tan, J.P. & Merrifield, R.B. (1981). Quantitative monitoring of solid phase peptide synthesis by the ninhydrin reaction. *Anal. Biochemistry* **117**, 147–157.
38. Marion, D. & Wüthrich, K. (1983). Application of phase sensitive two dimensional correlated spectroscopy (COSY) for measurement of ^1H–^1H spin–spin couplings in proteins. *Biochem. Biophys. Res. Comm.* **113**, 967–974.
39. Rance, M., Sørenson, O.W., Bodenhausen, G., Wagner, G., Ernst, R.R. & Wüthrich, K. (1983). Improved spectral resolution in COSY ^1H NMR spectra of proteins via double quantum filtering. *Biochem. Biophys. Res. Comm.* **117**, 479–485.
40. Braunschweiler, L. & Ernst, R.R. (1983). Coherence transfer by isotropic mixing: application to proton correlation spectroscopy. *J. Magn. Reson.* **53**, 521–528.
41. Bax, A. & Davis, D.G. (1985). MLEV-17 based two dimensional homonuclear magnetisation transfer spectroscopy. *J. Magn. Reson.* **65**, 355–360.
42. Greisinger, C., Sørenson, O.W. & Ernst, R.R. (1987). Practical aspects of the E.COSY technique: measurement of scalar spin-spin coupling constants in peptides. *J. Magn. Reson.* **88**, 177–185.
43. Kumar, A. Ernst, R.R. & Wüthrich, K. (1980). A two-dimensional nuclear Overhauser enhancement (2D NOE) experiment for elucidation of complete proton–proton cross relaxation networks in biological macromolecules. *Biochem. Biophys. Res. Comm.* **95**, 1–6.
44. Wagner, G. (1990). NMR investigations of protein structure. *Prog. NMR Spectroscopy* **22**, 101–139.
45. Nilges, M., Gronenborn, A.M., Brünger, A.T. & Clore, G.M. (1988). Determination of three-dimensional structures of proteins by simulated annealing with interproton distance constraints. Application to crambin, potato carboxypeptidase inhibitor and barley serine proteinase inhibitor 2. *Protein Eng.* **2**, 27–38.
46. Hoshi, T., Zagotta, W.N. & Aldrich, R.W. (1990). Biophysical and molecular mechanisms of *Shaker* potassium channel inactivation. *Science* **250**, 533–538.
47. Naranjo, D. & Miller, C. (1996). A strongly interacting pair of residues on the contact surface of charybdotoxin and a *Shaker* K^+ channel. *Neuron* **16**, 123–130.